PCCP

PAPER

View Article Online
View Journal | View Issue

Cite this: *Phys. Chem. Chem. Phys.*, 2014, **16**, 9403

Thermal boundary conductance between Al films and GaN nanowires investigated with molecular dynamics

Xiao-wang Zhou,[a] Reese E. Jones,*[a] Patrick E. Hopkins[b] and Thomas E. Beechem[c]

Received 17th January 2014,
Accepted 25th March 2014

DOI: 10.1039/c4cp00261j

www.rsc.org/pccp

GaN nanowires are being pursued for optoelectronic and high-power applications. In either use, increases in operating temperature reduce both performance and reliability making it imperative to minimize thermal resistances. Since interfaces significantly influence the thermal response of nanosystems, the thermal boundary resistance between GaN nanowires and metal contacts has major significance. In response, we have performed systematic molecular dynamics simulations to study the thermal boundary conductance between GaN nanowires and Al films as a function of nanowire dimensions, packing density, and the depth the nanowire is embedded into the metal contact. At low packing densities, the apparent Kapitza conductance between GaN nanowires and an aluminum film is shown to be larger than when contact is made between films of these same materials. This enhancement decreases toward the film–film limit, however, as the packing density increases. For densely packed nanowires, maximizing the Kapitza conductance can be achieved by embedding the nanowires into the films, as the conductance is found to be proportional to the total contact area.

1 Introduction

Gallium nitride (GaN) is of interest for electronic applications in light-emitting diodes and high power devices. GaN nanowires have unique advantages over conventional bulk forms of the material due to alterations in the bandstructure that occur with a reduction in dimension. Practically, these changes can improve the efficiencies of optoelectronics[1] and offer the promise of field effect transistors that operate in the quantum cascade limit.[2,3] Constructing a device necessitates that a nanowire make contact with other materials, in particular, to metal electrodes. In nanosystems, interfaces and, hence, these contacts have the potential to dictate the response of the device more than the constituent materials.[4] In fact, the nature of the contact interface between the nanowire and the electrodes can dominate the performance of the device. While past studies have examined the influence of contacts on the electrical response of nanowire devices,[5,6] the thermal resistance of metal contacts to nanowires remains largely unprobed. In response, we examine the nature of the thermal resistance between metal contacts and nanowires *via* a series of thermal molecular dynamics (MD) simulations.

In general, interfaces between different materials exhibit a high resistance to thermal transport.[7] This thermal interface resistance has been termed the Kapitza resistance, and its reciprocal the Kapitza conductance.[8,9] Within nanosystems, interfacial effects are of heightened importance due to the increased number of interfaces implicit with decreased device size and the likelihood of ballistic transport in a low-dimensional material. Thus, Kapitza resistance can become the dominant thermal resistance in a system. This has direct effects on device performance, in that: (a) electronic functionality usually deteriorates at excessive temperatures in GaN devices, and (b) a high Kapitza resistance has been reported to cause catastrophic failures of nanowire devices.[4,10–12]

Despite the significant impact of interfacial effects in nanowire devices, experimental studies of thermal transport between films and nanowires remain challenging. In contrast, molecular dynamics (MD) simulations have been successfully applied in recent years to understand the phenomena underlying Kapitza conductance.[13–26] In an MD simulation, atomic structures of nanowires are represented by an assembly of atoms connected by an interatomic potential. Thermal transport phenomena can be simulated by solving velocities (and hence temperature) of the atoms as a function of time from Newton's equations of motion under externally applied heat fluxes. The resulting evolution enables both calculation of Kapitza conductance

[a] *Mechanics of Materials Department, Sandia National Laboratories, Livermore, California 94550, USA. E-mail: rjones@sandia.gov*
[b] *Department of Mechanical and Aerospace Engineering, University of Virginia, Charlottesville, Virginia 22904, USA*
[c] *Nanoscale Sciences Department, Sandia National Laboratories, Albuquerque, New Mexico 87185, USA*

and fundamental analysis of such properties as the phonon density of states.[24] Here we perform MD simulations using LAMMPS[27] to gain an understanding of Kapitza resistance between Al films and GaN nanowires as a function of: nanowire dimensions, packing density, and the depth to which they are embedded within the metallic film. The lack of electron-mediated transport in this study should not impair our ability to obtain the sensitivity of conductance to various geometric factors since, as ref. 23 shows, the addition of these carriers does not have strong effects on the interface resistance if the coupling of electronic states in the conductor and phonons in the insulator is through lattice vibrations. This assumption is also supported by the work of Singh *et al.*[28] which finds that electron–phonon coupling is not a major contributor to thermal resistance across metal-dielectric interfaces at room temperature and above.†

Since thermal transport in a wire–film system has received little attention and yet this arrangement has many technologically relevant applications, we seek a fundamental understanding of the exact nature of interfacial thermal transport. After giving the details of the methods we use in Method section, we explore the dependence of the nanowire–film conductance to various geometric factors, including nanowire size and embedding depth in Results section in order to discover the strongest sensitivities. We find that some of the scaling effects are opposite to that typically observed in homogeneous materials.[12,20,31–34] In particular, nanostructuring appears to enhance the apparent conductance and may be a route to alleviating unacceptable interface resistance in devices. The reasons for this enhancement are discussed in detail in Discussion section and the results are summarized in Conclusion section.

2 Method

In this work, *direct method* MD simulations[22–24,33–37] were performed to calculate the thermal boundary conductance between an face-centered-cubic (FCC) Al film and a hexagonal wurtzite (Wz) GaN nanowire. The Al–Ga–N Stillinger–Weber (SW) potential found in ref. 22 was used to model the interactions. This potential is only one of a few potentials designed for a metal–semiconductor systems, *cf.* ref. 38–40, and is an extension of Béré and Serra's SW potential[41,42] for GaN. Despite overestimating the elastic constants of Al, see ref. 22, App. C, the predicted film-to-film conductance, 0.12 GW m^{-2} K^{-1}, compares well with the measurement of 0.19 GW m^{-2} K^{-1} reported in ref. 43. We believe the correspondence is due to the fact that different populations of phonons contribute significantly to conductivity in the pure phases *versus* the interface conductance, as demonstrated in our previous work.[23]

The orientations and dimensions of the computational crystals, composed of an Al film in contact with a GaN wire, are shown in Fig. 1. The GaN wire is either in simple end contact with the flat Al surface, or partially embedded in the Al film where a hexagonal hole of depth δ_i is created in the Al surface. A GaN nanowire with an additional length δ_i beyond its nominal, exposed length L_{GaN} is then created and embedded in the hole. Clearly, $\delta_i \to 0$ leads to the simple end contact configuration.

The equilibration procedure is essentially the same as in previous work.[22–24,33,34,36,37] First, a computational system with the desired dimensions is created based on the given 0 K temperature lattice constants of the Al and GaN crystals. To accommodate thermal expansion, a pre-conditioning simulation is performed for a total of 20 ps with periodic boundary

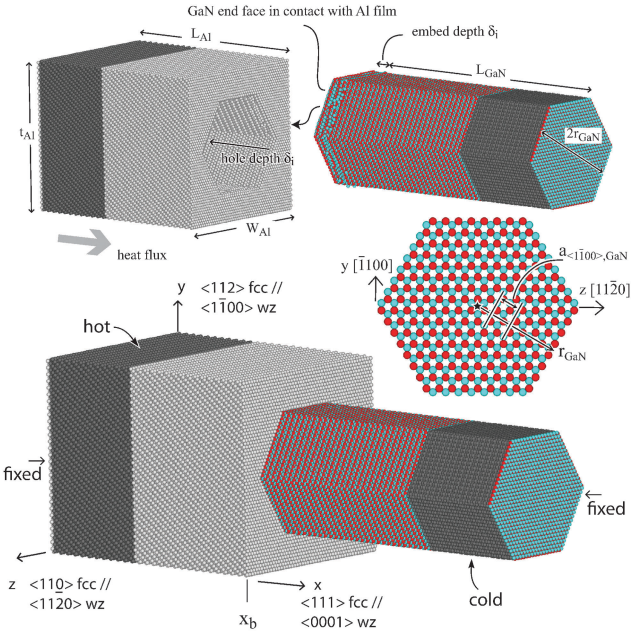

	Al film (FCC)	GaN wire (Wz)
lattice constant	a=0.405 (nm)	a=0.319 nm c=0.520 nm
basis	$x:\langle 111\rangle$ $y:\langle 112\rangle$ $z:\langle 110\rangle$	$x:\langle 0001\rangle$ $r:\langle 1\bar{1}00\rangle$
unit cell	$a_x = \sqrt{3}a = 0.701$ nm $a_y = \sqrt{3/2}a = 0.496$ nm $a_z = \sqrt{1/2}a = 0.286$ nm	$a_x = c = 0.502$ nm $a_r = \sqrt{3}/2a = 0.276$ nm
dimensions	$x: L = 16.824$ nm $y: t = n_y \cdot a_y$ $z: W = n_z \cdot a_z$	$x: L = 24.96$ nm $r: r = n_r \cdot a_r$

Fig. 1 Orientations and dimensions of the computational crystals. Note the heat flux is primarily in the x direction and the widths of the hot and cold reservoirs are the same. The radius of the wire is defined as the minimum distance between the center of the wire and the surface, *i.e.* the radius of the inscribed circle or the *apothem*, such that the cross-sectional area is $A_{GaN} = 2\sqrt{3}r_{GaN}^2$. The position, x_b, at which the temperature jump ΔT is evaluated in eqn (4) is at the left hexagonal "end" face of the GaN nanowire after embedding or surface contact with the Al film.

† The thermal direct coupling of metallic electrons and phonons in an insulator was postulated in ref. 29 and applied to a atomistic system in ref. 30 but has not had direct experimental confirmation to our knowledge.

conditions in all three coordinate directions using zero-pressure dynamics and velocity rescaling to effect the desired system temperature T. The time-averaged dimensions obtained during the last 10 ps are then used to create the system that is employed in the thermal transport simulation.

In the thermal transport simulation, periodic boundary conditions are used only in the y- and z-directions so that the simulated Al lattice approximates an infinite film and, as in previous work,[24] layers of atoms at the x ends fixed. In particular, one atomic Al layer at the left end and a pair of atomic Ga and N layers at the right end are frozen. Dynamics are run for 10 ps at a constant volume using velocity rescaling to maintain the desired system temperature; subsequently, the dynamics are changed to constant energy (and constant system volume) while a constant heat flux is introduced.[15,44–48] Two thermal reservoirs, comprised of $\approx$8.0 nm wide regions immediately next to the two fixed ends (the dark regions in Fig. 1), are used to create this flux.‡ A constant amount of kinetic energy Q is added to the hot region at the left and Q is removed from the cold region at the right at each time step, Δt, *via* velocity rescaling while preserving linear momentum.

This procedure creates a temperature differential across the computational region; but, due to the difference in cross-sectional area of the film, A_{Al}, and the wire, A_{GaN}, the mean flux into the cold reservoir and that out of the hot reservoir will not be equal. In fact, three flux definitions arise from the chosen geometry: (a) the flux with respect to the cross-sectional area of the GaN wire A_{GaN},

$$J \equiv \frac{Q}{\Delta t A_{\mathrm{GaN}}}; \tag{1}$$

(b) the flux with respect to the cross-sectional of the Al film A_{Al}, $J_{\mathrm{Al}} \equiv Q/\Delta t A_{\mathrm{Al}}$; and (c) that with respect to the full embedded area of the interface,

$$A_{\mathrm{interface}} = \underbrace{2\sqrt{3}r_{\mathrm{GaN}}^{2}}_{A_{\mathrm{GaN}}} + \underbrace{4\sqrt{3}r_{\mathrm{GaN}}\delta_i}_{A_i} \tag{2}$$

$J_{\mathrm{interface}} = Q/\Delta t A_{\mathrm{interface}}$. For concreteness, we reference the Kapitza estimates to J, since this is the apparent conductance with respect to the nanowire, and use a value of 20.0 eV ns^{-1} nm^{-2} for all simulations. Hence, the other two fluxes will change as the film geometry and embedding depth, δ_i, change, even though J is held fixed.

After waiting 0.4 ns to allow the system to reach a steady state, the average temperature profile is computed with 40 finite elements along the x-direction. A temperature at each node is defined from the kinetic energy of all the atoms within the support of and weighted by the node's piecewise-linear basis function and averaged over all the steady-state time-steps. To reduce statistical fluctuations of the results, the duration of the constant energy/steady flux simulations is at least 11 ns. For similar reasons, all simulations are performed at T = 300 K even though this temperature is not necessarily above the system's Debye temperature to reduce statistical noise. We emphasize that: (a) our objective is to understand the effects of nanowire dimension on Kapitza resistance rather than to extract quantitative predictions, and (b) the reduced systematic/statistical errors resulting from low temperature simulations are crucial for drawing reliable conclusions with limited computational resources.[33,34,37] Also, we note that the Kapitza resistance linearly scales with the inverse of sample length,[23] at least in a film-to-film arrangement. Hence, utilization of a sufficiently large system dimension to produce size insensitive results is computationally impractical. With this understood, we explore systems with fixed sample length, see Table 1. The chosen length will affect the quantitative results, but will not influence the qualitative trends that are the goal of this study. In addition, the lengths selected, L_{Al} = 16.8 nm and L_{GaN} = 25.0 nm, are on par with technologically relevant device sizes.[49]

‡ Note that the number of atoms in the cold region (GaN wire) is smaller than in the hot region (Al film) due to the choice to make the reservoirs have the same width in the flux direction.

Table 1 Four series of system dimensions explored with fixed $n_{x,\mathrm{Al}}$ = 24 and $n_{x,\mathrm{GaN}}$ = 48. For series 1, 2, 4 the area of the Al film is fixed at $A_{\mathrm{Al}} = n_{y,\mathrm{Al}} \times n_{z,\mathrm{Al}}$ = 29 × 49

1: End contact δ_i = 0 nm, varying radius:						
$n_{r,\mathrm{GaN}}$	6	8	10	12	14	16
2: Embedded wire δ_i = 1 nm, varying radius:						
$n_{r,\mathrm{GaN}}$	6	8	10	12	14	16
3: End contact, constant radius $n_{r,\mathrm{GaN}}$ = 6, varying film area:						
A_{Al}	8 × 14		16 × 28		29 × 49	
4: Constant radius wire $n_{r,\mathrm{GaN}}$ = 12, varying embedded depth:						
δ_i [nm]	0.0000	0.0806	0.2602	0.5204	0.7806	1.0413

The Kapitza conductance h is then calculated as:

$$h = \frac{J}{\Delta T} = \frac{Q}{\Delta t A_{\mathrm{GaN}} \Delta T}, \tag{3}$$

where J is the heat flux, defined in eqn (1), and ΔT is the abrupt temperature change at the interface estimated from the temperature profiles of the film and wire as

$$\Delta T = [T_{\mathrm{Al}}(x) - T_{\mathrm{GaN}}(x)]_{x=x_b} \tag{4}$$

where $T_{\mathrm{Al}}(x)$ and $T_{\mathrm{GaN}}(x)$ are linear fits to the temperature profiles slightly away from the jump and x_b is the position of the (vertical) material boundary *i.e.* the location of the end contact with cross-section A_{GaN}, refer to Fig. 1. The rationale for this definition is: the temperature contours become flat and aligned perpendicular to the flux direction (x) away from the material interface between the film and wire. The temperature profiles in Fig. 2 and the temperature map in Fig. 3 in part, validate this rationale and will be discussed in more detail in the next section. Also this definition, unlike a conductance resolved to and defined on the atomic scale along the material interface, is accessible to experiment, and consistent with our previous work.[24]

3 Results

To determine the influence of the size, packing density, and the embedded depth of the wires on boundary conductance we use

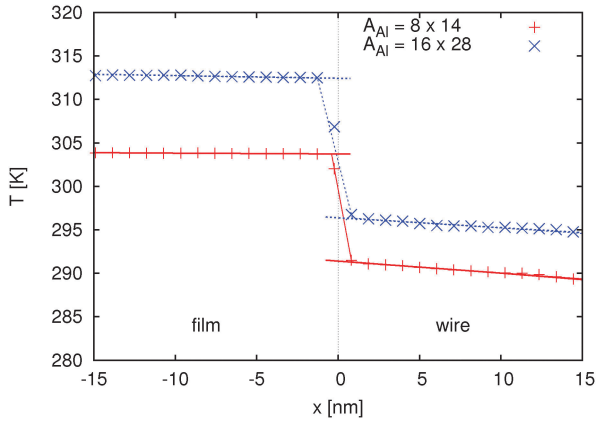

Fig. 2 Typical temperature profiles at a heat flux of J = 20.0 eV ns^{-1} nm^{-2} for GaN wires with radius r_{GaN} = 1.7 nm and contacting periodic Al films with two different cross-sectional areas. The temperature jump ΔT is calculated from the difference in the linear fits of the two bulk regions evaluated at the (vertical) material interface of the end of the nanowire using eqn (4).

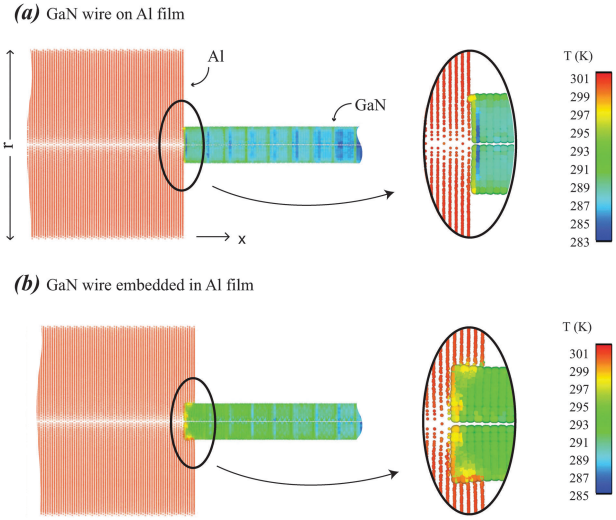

Fig. 3 Temperature map in x- and r-directions with GaN wire radius $n_{r,GaN}$ = 6 for: (a) an end-contacted GaN wire, and (b) an embedded GaN. Here the color scheme indicates temperature, with the small spheres depicting Al atoms, and large spheres depicting Ga and N atoms. Note: (1) to decrease noise, the temperatures of all atoms at the same r coordinate have been averaged together; (2) the white region at r = 0 is due to the lack of atoms to sample when $r \to 0$; and (3) there is a slight visible modulation of temperature in the GaN wire likely due to the non-equilibrium nature of the simulation.

four parametric studies, enumerated in Table 1. In the first series, the thermal boundary conductance h is examined as a function of GaN nanowire radius, r_{GaN}, for end contact (δ_i = 0) of the nanowire with the film. In the second series, the wire is embedded into the film δ_i = 1.0 nm and the simulations are conducted with the same sequence of radii. In the third series, we change the cross-sectional area of the Al film, A_{Al}, while keeping the nanowire radius fixed. Under lateral periodic boundary conditions, this essentially changes the packing density of the nanowires, in units of nanowire/A_{Al} or A_{GaN}/A_{Al}.

To further elucidate the effect of embedding the nanowires we assess the thermal boundary conductance at different embedded depths, δ_i, in the fourth series while keeping the other dimensions fixed.

3.1 Temperature field

To ensure that temperature fields sufficiently smooth to utilize eqn (3) exist, we examined the temperature profile along the primary flux direction and across the interface. Fig. 2 shows typical temperature profiles for two systems with same radius wire, $n_{r,GaN}$ = 6, but with different film areas, A_{Al}. As expected from a system with significant interfacial resistance, Fig. 2 shows an abrupt temperature change at the Al:GaN interface; whereas, the temperature changes within both the Al region and the GaN region are linear and relatively small. The linearity of the temperature profiles in the two materials is indicative of primarily diffusive transport. We used a small heat flux, J = 20.0 eV ns^{-1} nm^{-2}, to remain close to the linear response regime where the Kapitza conductance h is a valid measure; however, this prevents the simultaneous deduction of thermal conductivities, $\kappa = J/\nabla T$, for GaN and Al due to the small temperature gradients within the constituent materials. Also, the effect of electron-mediated heat transport in the Al film would only further flatten the temperature profile on the Al side. In addition, as ref. 23 shows, electron-mediated transport in a metallic-insulator system does not have strong effects on the interface resistance if the coupling of electronic states in the conductor and phonons in the insulator is through lattice vibrations.

Fig. 3 provides a more detailed, atom-by-atom map of the temperature for an embedded nanowire and an end-contacted wire. As can be seen, regardless of the type of contact, the temperature profile along the radial direction is relatively uniform in the entire system. Furthermore, the temperature gradient along the axial, x-direction is relatively small in both the Al and the GaN. There are variations in the temperature jump along the end face and the modulation in temperature along the GaN wire but they are minimal. Taken together, this implies that: (a) the end and lateral faces have approximately the same jump in temperature over the entire embedded length, and (b) the flux near the contact is approximately perpendicular to the surface *i.e.* in the r-direction on the lateral faces. This observation gives further motivation for the definition of h in eqn (3) and is the basis for an upcoming discussion of how anisotropy affects the apparent conductance.

3.2 Packing density

In three different studies, (1) varying the radius of an end-contacted wire, (2) varying the radius of an embedded wire, and (3) the lateral extent of the film contacting the end of a fixed size wire, we changed the relative cross-sectional areas of the wire, A_{GaN}, *vs.* film, A_{Al}, and hence the packing density of the periodic images of the wires. The calculated apparent conductance values are shown in Fig. 4 as a function of the area ratio, A_{GaN}/A_{Al}. For smaller cross-sectional areas A_{GaN}, the statistical error is larger due to the reduced number of Ga and N atoms

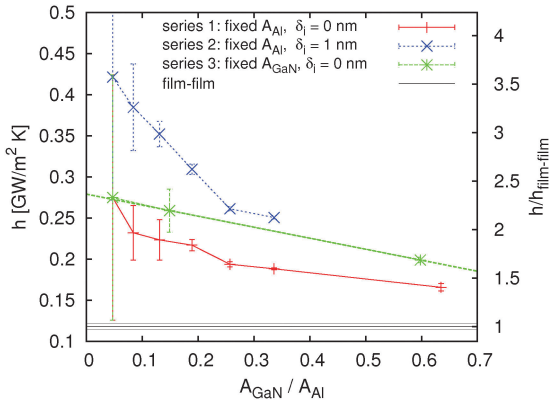

Fig. 4 Kapitza conductance as a function of GaN-to-Al area ratio. The red line shows the trend for end-contacted wires of varying cross-section (series 1), the blue line shows the trend for wires of varying cross-section and a fixed embedded depth (series 2), and the green data is for systems with different A_{Al} areas (series 3). All three datasets approach the Al film–GaN film conductance limit for an GaN film of approximately the same thickness as the length of the GaN wire. This limit, $h_{\mathrm{Al\,film-GaN\,film}} \equiv \lim_{A_{GaN}\to A_{Al}} h = 0.118 \pm 0.003\,\mathrm{GW\,m^{-2}\,K^{-1}}$ at the chosen L_{GaN} and L_{Al}, is depicted with thin black lines. Also, for series 3 (green data) where the area of the film A_{Al} is varying, the limit for a laterally infinite film of the given thickness and a single, isolated wire can be estimated *via* extrapolation: $\lim_{A_{Al}\to\infty} h = 0.279\,\mathrm{GW^{-1}\,m^{-2}\,K^{-1}}$.

used in the calculation of average temperatures.§ Nevertheless, the data convincingly shows that the Kapitza conductance h increases as the packing density of the nanowire decreases. In fact, the Kapitza conductance between the end-contacted GaN wire and Al film can be a few times larger than that of a film to film contact of the same materials, refer to Fig. 4. If the nanowire is embedded within the Al contact, this effect becomes even more pronounced in that the apparent Kapitza conductance of an embedded nanowire, as defined in eqn (3), increases relative to a nanowire making only end contact as shown in Fig. 4. If the lateral area of the film is varied, as in the third data series, the trend is similar albeit without the change in slope displayed by the first two series.

Despite no exact master curve with respect to the area ratio, A_{GaN}/A_{Al}, a number of limits are apparent from these three parameter studies. First, the linearity of the series 3 data shown in Fig. 4 allows for extrapolation of estimate interfacial conductance of the limiting case of a single isolated wire with some confidence. For the given film depth and wire dimensions ($n_{r,GaN} = 12$), $\lim_{A_{Al}\to\infty} h = 0.279\,\mathrm{GW^{-1}\,m^{-2}\,K^{-1}}$ which is considerably greater than the corresponding film–film value $h_{\mathrm{Al\,film-GaN\ film}} = 0.118\,\mathrm{GW\,m^{-2}\,K^{-1}}$ calculated separately. In general, all three cases appear to approach this film–film conductance as $A_{GaN}/A_{Al}\to 1$ but the approach does not appear entirely uniform. Perhaps to attain a master curve and an asymptotic approach to the film–film limit both the wire and the film must be considerably larger in lateral extent.

§ A similar approach to that described previously in ref. 37 is used to estimate the standard deviation of the Kapitza conductance.

At first glance, the overall enhancement is counter-intuitive considering that smaller nanostructures tend to have decreased thermal conductivity due to phonon boundary scattering[33,34] or diffraction limited transport through constrictions.[50] Here, the opposite is observed. These trends are also in contrast to previous findings[23] that the periodic area does not affect Kapitza conductance of multilayer films. Thus, any changes in h observed, particularly in the third series, are due to physical phenomena associated with a film–nanowire contact and not an artificial finite-size effect.

3.3 Embedded depth and anisotropy

Results of the fourth series, for wire–film systems with different embedded depths and fixed GaN wire radius, are shown in Fig. 5. It indicates that the Kapitza conductance increases linearly with the embedded depth, supporting the hypothesis that in certain regimes the Kapitza conductance is proportional to the total contact area between Al and GaN nanowire as in our previous work on interfacial morphology.[24] On the other hand, Fig. 5 shows that the conductance referenced to the total interfacial area, $A_{\mathrm{interface}}$, actually decreases slightly with increased embedding. A linear equation for Kapitza conductance h as a function of the embedded depth δ_i can be derived:

$$h = h_x + \frac{A_i}{A_{\mathrm{GaN}}} h_r = h_x + \frac{2h_r}{r_{\mathrm{GaN}}} \cdot \delta_i \qquad (5)$$

based on conservation of total heat flux and assuming a uniform temperature drop across the interface, where h_x and h_r are, respectively, the local Kapitza conductances in the x- and r-directions. By fitting eqn (5) to the MD data we inferred h_x = 0.22 GW m^{-2} K^{-1} and h_r = 0.14 GW m^{-2} K^{-1}. The fact that transmission is apparently less efficient through the lateral faces than through the end face of the wire in this arrangement is consistent with the decreasing trend of $h_{\mathrm{interface}}$ in Fig. 5.

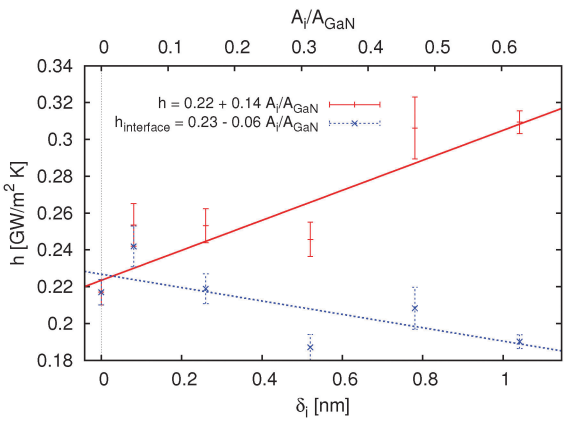

Fig. 5 Apparent Kapitza conductance h as a function of embedded depth δ_i (or lateral embedded area $A_i = 4\sqrt{3} r_{\mathrm{GaN}} \delta_i$) of the GaN nanowire referenced to A_{GaN} using eqn (5) and $h_{\mathrm{interface}} = \dfrac{Q}{\Delta t A_{\mathrm{interface}} \Delta T}$ referenced to the interface area $A_{\mathrm{interface}} = A_i + A_{\mathrm{GaN}}$ defined in eqn (2). Based on the variance-weighted linear regression of the series 4 data $h_r/h_x \approx 0.61$.

4 Discussion

In addition to the anisotropy in conductance, our studies indicate that the apparent Kapitza conductance is higher for the contact between a film and a narrow wire than film-to-film, and this improvement is increased when: (a) the wire is embedded in the film, (b) the radius of the wire is decreased leading to low packing densities, and (c) the area of Al film is increased, also leading to low wire packing density. The former phenomenon seems to be primarily a result of total area of contact, given the specularity of the interface. In this section we seek to better understanding of the anisotropy and the latter two phenomena.

4.1 Anisotropy

We believe the anisotropy of h_x and h_r is a clear consequence of the wurtzite structure of GaN. Previously, it has been shown both experimentally[51] and with MD[52] that the orientation of a hexagonal crystal structure relative to the interface can significantly alter the transport across the interface. This is primarily due to differences in the size of the Brillouin zone and magnitudes of the group velocities, v_i, along the different (propagation) directions of a non-cubic crystal. Quantitatively, it has been shown that the ratio of the thermal boundary conductance along the different directions, h_x/h_r, is approximately equivalent to the ratio of the Brillouin zone averaged group velocities, $\bar{v}_x/\bar{v}_r$. In the classical limit, $\bar{v}_i$, $i \in \{x,r\}$ is defined as:

$$\bar{v}_i = \sum_j \frac{k_B T}{\Delta k_{i,j} \hbar} \int \frac{v_{i,j}(k)}{\omega(k)} \mathrm{d}k. \quad (6)$$

Here, the summation takes place over all polarizations, j, but the integration is performed over only those wavevectors k corresponding to frequencies ω that exist within the other material making up the interface,[51] in this case the Al. Also, $\Delta k_{i,j}$ is the width of the Brillouin zone for the particular propagation i and polarization j branch, and k_B is the Boltzmann constant. With eqn (6), we calculated the averaged group velocities of GaN along $\overrightarrow{\Gamma A}$ and $\overrightarrow{\Gamma M}$, since these directions are parallel to the conductance in the x- and r-directions, respectively. Using 4th order polynomial fits[53,54] to represent the GaN dispersion calculated by Ruf *et al.*,[55] eqn (6) gives $\bar{v}_r/\bar{v}_x$ = 0.53. This value compares well to the ratio h_r/h_x = 0.61 inferred with eqn (5). Hence we conclude that anisotropic effects, in addition to interfacial area, in large part determine the transport efficiency of the embedded nanowires.¶ Since the group velocities in the two directions for GaN are comparable, the main effect is due to difference in length of the Brillouin zone along $\overrightarrow{\Gamma A}$ and $\overrightarrow{\Gamma M}$ directions together with the uniform density of modes.

4.2 Enhancement

With regard to conductivity (as opposed to interface conductance), the common conception[57] is that surface scattering and a size-dependent DOS are the primary mechanisms for size effects at the nanoscale. To this end, we examined the local density of states (LDOS) of vertical monolayers of atoms near the contact as an indication of the dispersion relation underlying the phonon transport. The density of states for a set of atoms of a single atomic type is given by the velocity correlation:

$$\mathrm{DOS}(\omega) = n \left| \mathscr{F}_{t\to\omega} \frac{\langle \mathbf{v}(0)\cdot\mathbf{v}(t)\rangle}{\langle \mathbf{v}(0)\cdot\mathbf{v}(0)\rangle} \right| = \frac{\rho}{2k_B T} \left| \mathscr{F}_{t\to\omega} \langle \mathbf{v}(0)\cdot\mathbf{v}(t)\rangle \right| \quad (7)$$

where: $\mathbf{v}$ is an atomic velocity, $\mathscr{F}_{t\to\omega}$ is the Fourier transform, n is the number density, ρ is the mass density and $3nk_BT = \rho\langle \mathbf{v}\cdot\mathbf{v}\rangle$ is the thermal energy density.[24,58]

Fig. 6, compares the LDOS for layers of atoms of: a given wire (r_{GaN} = 6) in end contact with two films of different lateral extent (upper), and a given film ($n_{y,Al} \times n_{z,Al}$ = 16 × 28) in end contact with two wires with different radii (lower).‖ Clearly, the two films in contact with identical wires have virtually the same LDOS despite one film having four times the lateral extent of the other. Also, only the layer directly adjacent to the GaN wire significantly deviates from the LDOS deeper in the Al. This implies that the films are acting in essentially isolated fashion and is corroborated by the fact that we can estimate the conductance of an isolated wire using series 3 in Fig. 4. Furthermore, the states at the free surface of the Al (*i.e.* the surface not covered by the wire) are essentially identical to the interior states, and hence distinct from the Al monolayer next to the wire.** This finding implies that: (a) the DOS of Al film is affected by the contact with wire in a abrupt and three-dimensional way, and (b) the main effects on conductance are

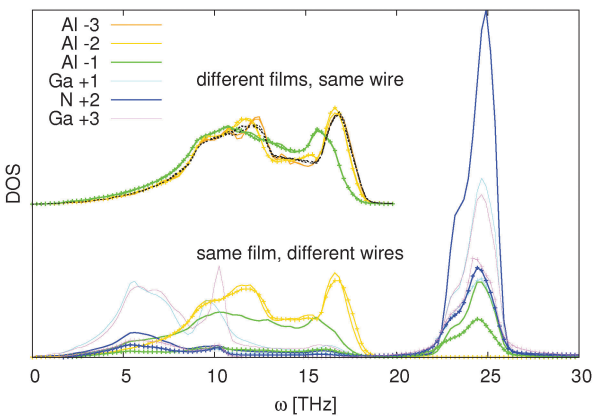

Fig. 6 Local density of states in layers near the interface, where layer −1 is the film monolayer closest to the interface and layer +1 is the wire monolayer closest to the interface. The sample boxes contain approximately 30 atoms per monolayer and the DOS is in arbitrary units. Upper graph: comparison of the same wire (r_{GaN} = 6) in end contact with films of small ($n_{y,Al} \times n_{z,Al}$ = 8 × 14, lines) and large ($n_{y,Al} \times n_{z,Al}$ = 16 × 28, lines with data points) cross-sectional areas, respectively. Only the film layers are shown for clarity and the overlapping black lines are the DOS of corresponding layers (−3, −2, −1) near the surface of the Al but away from the wire. Lower graph: comparison of a smaller GaN wire (r_{GaN} = 6, lines) and a larger wire (r_{GaN} = 12, lines with data points) contacting the same Al film with area $n_{y,Al} \times n_{z,Al}$ = 16 × 28.

¶ A differential in the adhesion strength of the end *versus* lateral interfaces is a possible correlated effect. A weaker interface bond has been shown to decrease conductance, see ref. 56.

‖ The calculated results can be compared to Fig 1(b) of ref. 59 which measures the partial DOS for Ga and N individually.

** The fact the LDOS at the free surface of the Al is identical to the interior states is likely an artifact of the nearest neighbor nature of the SW potential, refer to ref. 31.

solely due to deviations in the first layer of the film in contact with the wire, the extent of which is determined by the wire radius, and in the wire itself.

The lower graph of Fig. 6 shows a trace of LDOS across the interface. It clearly indicates the first layer of Al is depleted in the acoustic range and that optical-like modes also appear, as in ref. 22. Most importantly, it shows for the system with the larger wire the low frequency band is depleted relative to the smaller wire and this relative depletion extends one monolayer into the Al. This pattern is similar to that of the small *vs.* large film LDOS comparison (omitted for clarity from the upper graph) as the similarity of conductance with packing density (A_{GaN}/A_{Al}) trends in Fig. 4 indicates; however, since response in Fig. 4 does not collapse onto a master curve the pattern in DOS in Fig. 6 is only qualitatively similar.

Given earlier work[22,52,56] showing the correlation of conductance to overlap in the LDOS and its relationship to the more detailed direct investigation of the dispersion,[31] we can interpret these results in the same light. The reduction in the low frequency band especially with larger wire size (relative to the film) leads to lower conductance. Although the higher frequency band can transmit heat through the interface,[31] it is the low frequency modes that are the primary conduits.[60] The relative depletion of low frequency phonons in the larger wire, shown in Fig. 6, also correlates well with the finding[12] (Fig. 2) that the larger wires are less efficient in conducting heat in the end-contact with film configuration.

We also considered a related concept in attempting to explain the enhanced transport with decreased packing density: the increased efficiency of injecting phonons by virtue of the geometry of the three dimensional film:quasi-one dimensional wire system. As mentioned, the small differences in the edges of the contact *versus* the interior of the contact area, as manifest in the temperature map (Fig. 3), may indicate that phonons near the edge of contact can be injected, on average, with propagation directions that are not parallel to the net flow of heat even in the end-contacted case. This mode of enhancement has analogs with a continuum heat solution with a similar geometry, where the relative area of the nanowire with respect to that of the film A_{GaN}/A_{Al} changes the local flux distribution.

To test this hypothesis we created a GaN-only system with essentially the same dimensions as our base model ($n_{y,Al} \times n_{z,Al} = 16 \times 28$ and $r_{GaN} = 12$). No appreciable temperature jump and, hence, no measurable Kapitza resistance is seen in this system (calculated but not shown). This also implies that there is no possibility of enhancement over the film–film case and that a three-dimensional injection effect does not seem to be a primary mechanism for the enhancement. Nevertheless, the LDOS of the GaN film–GaN wire has variations from the interior of the film through the interface to the wire, and, in fact, the high-frequency band displays a region of depletion in the wire near the contact (not shown). Although Becker *et al.*[31] have shown that the high frequency band can contribute to thermal transport, our work[60] indicates that the low frequency modes transport most of the heat through an interface. From this it is possible to conclude that the depletion of LDOS near the contact for dispersion matched materials with perfect band overlap, as in this GaN film–GaN wire case, can lead to negligible interface resistance.

5 Conclusions

Large scale molecular dynamics scaling studies were used to investigate the Al film:GaN nanowire thermal boundary conductance and resulted in the following findings:

(a) In the presence of a heat flux, the temperature in the interior of the Al film is extremely uniform (see Fig. 2). While showing some gradient in the *x*-direction, the temperature in the GaN nanowire is also extremely uniform in the *r*-direction (refer to Fig. 3).

(b) Kapitza conductance with respect to the cross-sectional area of the wire for an end-contacted GaN nanowire and an Al film is significantly higher than that between GaN and Al films (see Fig. 4).

(c) Kapitza conductance decreases with increasing nanowire cross-section area and increasing nanowire packing density or the GaN-to-Al area ratio (refer again to Fig. 4). The two effects are correlated for a given Al cross-section area, since increasing nanowire cross-section area necessarily results in an increase in nanowire packing density.

(d) Although the scaling of conductance with the area ratio A_{GaN}/A_{Al} is not perfect, the isolated wire and film–film limits are apparent.

(e) The Kapitza conductance with respect to the cross-sectional area of the wire increases linearly with increasing embedded depth of the nanowire, supporting that the contact conductance is proportional to the total contact area for specular interfaces albeit with an orientation dependent coefficient (see Fig. 5).

As the work of Becker *et al.*[31] indicates, the transmission characteristics underlying the interface conductance are complex and deserve further detailed study to exploit the thermal properties of the film–nanowire system.

Acknowledgements

Sandia National Laboratories is a multi-program laboratory managed and operated by Sandia Corporation, a wholly owned subsidiary of Lockheed Martin Corporation, for the U.S. Department of Energy's National Nuclear Security Administration under contract DE-AC04-94AL85000. This work was performed under a Laboratory Directed Research and Development (LDRD) project. PEH is also appreciative for funding from the Office of Naval Research Young Investigator Program (N00014-3-0528) and support from the Commonwealth Research Commercialization Fund of Virginia.

References

1 Y. Xia, P. Yang, Y. Wu, B. Mayers, B. Gates, Y. Yin, F. Kim and H. Yan, *Adv. Mater.*, 2003, **15**, 353–389.
2 M. A. Khayer and R. K. Lake, *J. Appl. Phys.*, 2010, **107**, 014502.
3 M. A. Khayer and R. K. Lake, *J. Appl. Phys.*, 2010, **108**, 104503.
4 E. Pop, *Nano Res.*, 2010, **3**, 147–169.
5 C. Y. Chang, G. C. Chi, W. M. Wang, L. C. Chen, K. H. Chen, F. Ren and S. J. Pearton, *J. Electron. Mater.*, 2006, **35**, 738–743.
6 E. Stern, G. Cheng, E. Cimpoiasu, R. Klie, S. Guthrie, J. Klemic, I. Kretzschmar, E. Steinlauf, D. Turner-Evans, E. Broomfield, J. Hyland, R. Koudelka, T. Boone, M. Young, A. Sanders, R. Munden, T. Lee, D. Routenberg and M. A. Reed, *Nanotechnology*, 2005, **16**, 2941–2953.
7 P. E. Hopkins, *ISRN Mech. Eng.*, 2013, **2013**, 682586.

8 P. L. Kapitza, *J. Phys.*, 1941, **4**, 181–210.
9 E. T. Swartz and R. O. Pohl, *Rev. Mod. Phys.*, 1989, **61**, 605–668.
10 D. G. Cahill, W. K. Ford, K. E. Goodson, G. D. Mahan, A. Majumdar, H. J. Maris, R. Merlin and S. R. Phillpot, *J. Appl. Phys.*, 2003, **93**, 793–818.
11 T. Westover, R. Jones, J. Huang, G. Wang, E. Lai and A. A. Talin, *Nano Lett.*, 2008, **9**, 257–263.
12 Y. Chalopin, J.-N. Gillet and S. Volz, *Phys. Rev. B: Condens. Matter Mater. Phys.*, 2008, **77**, 233309.
13 E. S. Landry and A. J. H. McGaughey, *Phys. Rev. B: Condens. Matter Mater. Phys.*, 2009, **80**, 165304.
14 M. Hu, P. Keblinski and P. K. Schelling, *Phys. Rev. B: Condens. Matter Mater. Phys.*, 2009, **79**, 104305.
15 P. K. Schelling, S. R. Phillpot and P. Keblinski, *J. Appl. Phys.*, 2004, **95**, 6082–6091.
16 Z.-Y. Ong and E. Pop, *Phys. Rev. B: Condens. Matter Mater. Phys.*, 2010, **81**, 155408.
17 S. Shin, M. Kaviany, T. Desai and R. Bonner, *Phys. Rev. B: Condens. Matter Mater. Phys.*, 2010, **82**, 081302R.
18 R. J. Stevens, L. V. Zhigilei and P. M. Norris, *Int. J. Heat Mass Transfer*, 2007, **50**, 3977–3989.
19 R.J. Stevens, P. M. Norris and L. V. Zhigilei, *Proc. IMECE04*, 2004, p. 60334.
20 S. Merabia and K. Termentzidis, *Phys. Rev. B: Condens. Matter Mater. Phys.*, 2012, **86**, 094303.
21 K. Termentzidis, J. Parasuraman, C. A. D. Cruz, S. Merabia, D. Angelescu, F. Marty, T. Bourouina, X. Kleber, P. Chantrenne and P. Basset, *Nanoscale Res. Lett.*, 2011, **6**, 288.
22 X. W. Zhou, R. E. Jones, J. C. Duda and P. E. Hopkins, *Phys. Chem. Chem. Phys.*, 2013, **15**, 11078–11087.
23 R. E. Jones, J. C. Duda, X. W. Zhou, C. J. Kimmer and P. E. Hopkins, *Appl. Phys. Lett.*, 2013, **102**, 183319.
24 X. W. Zhou, R. E. Jones, C. J. Kimmer, J. C. Duda and P. E. Hopkins, *Phys. Rev. B: Condens. Matter Mater. Phys.*, 2013, **87**, 094303.
25 D. R. Clarke and S. R. Phillpot, *Handbook of Nanoscience, Engineering, and Technology*, CRC Press, 3rd edn, 2012, ch. 19, pp. 545–572.
26 A. McGaughey, *Annu. Rev. Heat Transfer*, DOI: 10.1615/AnnualRevHeatTransfer.2013006915.
27 S. J. Plimpton, Sandia National Laboratories, 2010, http://lammps.sandia.gov.
28 P. Singh, M. Seong and S. Sinha, *Appl. Phys. Lett.*, 2013, **102**, 181906.
29 A. Majumdar and P. Reddy, *Appl. Phys. Lett.*, 2004, **84**, 4768–4770.
30 Y. Wang, X. Ruan and A. K. Roy, *Phys. Rev. B: Condens. Matter Mater. Phys.*, 2012, **85**, 205311.
31 B. Becker, P. K. Schelling and S. R. Phillpot, *J. Appl. Phys.*, 2006, **99**, 123715.
32 B. Poudel, Q. Hao, Y. Ma, Y. Lan, A. Minnich, B. Yu, X. Yan, D. Wang, A. Muto and D. Vashaee, *et al.*, *Science*, 2008, **320**, 634–638.
33 X. W. Zhou, R. E. Jones and S. Aubry, *Phys. Rev. B: Condens. Matter Mater. Phys.*, 2010, **81**, 073304.
34 X. W. Zhou, R. E. Jones and S. Aubry, *Phys. Rev. B: Condens. Matter Mater. Phys.*, 2010, **81**, 155321.
35 J. C. Duda, C. J. Kimmer, W. A. Soffa, X. W. Zhou and R. E. Jones, *J. Appl. Phys.*, 2012, **112**, 093515.
36 X. W. Zhou and R. E. Jones, *Modell. Simul. Mater. Sci. Eng.*, 2011, **19**, 25004.
37 X. W. Zhou, S. Aubry, R. E. Jones, A. Greenstein and P. K. Schelling, *Phys. Rev. B: Condens. Matter Mater. Phys.*, 2009, **79**, 115201.
38 K. Albe, K. Nordlund and R. S. Averback, *Phys. Rev. B: Condens. Matter Mater. Phys.*, 2002, **65**, 195124.
39 X. Zhou, H. Wadley, J.-S. Filhol and M. Neurock, *Phys. Rev. B: Condens. Matter Mater. Phys.*, 2004, **69**, 035402.
40 S. Wang and H. Ye, *Curr. Opin. Solid State Mater. Sci.*, 2006, **10**, 26–32.
41 A. Béré and A. Serra, *Phys. Rev. B: Condens. Matter Mater. Phys.*, 2002, **65**, 205323.
42 A. Béré and A. Serra, *Philos. Mag.*, 2006, **86**, 2159–2192.
43 R. J. Stevens, A. N. Smith and P. M. Norris, *J. Heat Transfer*, 2005, **127**, 315–322.
44 T. Ikeshoji and B. Hafskjold, *Mol. Phys.*, 1994, **81**, 251–261.
45 P. K. Schelling and S. R. Phillpot, *J. Am. Ceram. Soc.*, 2001, **84**, 2997–3007.
46 P. Jund and R. Jullien, *Phys. Rev. B: Condens. Matter Mater. Phys.*, 1999, **59**, 13707–13711.
47 P. K. Schelling, S. R. Phillpot and P. Keblinski, *Phys. Rev. B: Condens. Matter Mater. Phys.*, 2002, **65**, 144306.
48 Y. G. Yoon, R. Car, D. J. Srolovitz and S. Scandolo, *Phys. Rev. B: Condens. Matter Mater. Phys.*, 2004, **70**, 012302.
49 K. S. Novoselov, A. K. Geim, S. V. Morozov, D. Jiang, Y. Zhang, S. V. Dubonos, I. V. Grigorieva and A. A. Firsov, *Science*, 2004, **306**, 666–669.
50 R. Prasher, T. Tong and A. Majumdar, *Appl. Phys. Lett.*, 2007, **91**, 143119.
51 P. E. Hopkins, T. Beechem, J. C. Duda, K. Hattar, J. F. Ihlefeld, M. A. Rodriguez and E. S. Piekos, *Phys. Rev. B: Condens. Matter Mater. Phys.*, 2011, **84**, 125408.
52 J. Duda, C. Kimmer, W. Soffa, X. Zhou, R. Jones and P. Hopkins, *J. Appl. Phys.*, 2012, **112**, 093515.
53 J. C. Duda, T. E. Beechem, J. L. Smoyer, P. M. Norris and P. E. Hopkins, *J. Appl. Phys.*, 2010, **108**, 073515.
54 T. Beechem, J. C. Duda, P. E. Hopkins and P. M. Norris, *Appl. Phys. Lett.*, 2010, **97**, 061907.
55 T. Ruf, J. Serrano, M. Cardona, P. Pavone, M. Pabst, M. Krisch, M. D'astuto, T. Suski, I. Grzegory and M. Leszczynski, *Phys. Rev. Lett.*, 2001, **86**, 906.
56 J. C. Duda, T. S. English, E. S. Piekos, W. A. Soffa, L. V. Zhigilei and P. E. Hopkins, *Phys. Rev. B: Condens. Matter Mater. Phys.*, 2011, **84**, 193301.
57 N. Mingo, L. Yang, D. Li and A. Majumdar, *Nano Lett.*, 2003, **3**, 1713–1716.
58 J. C. Duda, T. S. English, E. S. Piekos, W. A. Soffa, L. V. Zhigilei and P. E. Hopkins, *Phys. Rev. B: Condens. Matter Mater. Phys.*, 2011, **84**, 193301.
59 J. Nipko, C.-K. Loong, C. Balkas and R. Davis, *Appl. Phys. Lett.*, 1998, **73**, 34–36.
60 R. Jones, J. Duda, X. Zhou, C. Kimmer and P. Hopkins, *Appl. Phys. Lett.*, 2013, **102**, 183119.

